Nodal spin density wave and band topology of the FeAs-based materials

Ying Ran, Fa Wang, Hui Zhai, Ashvin Vishwanath, and Dung-Hai Lee
Department of Physics, University of California at Berkeley, Berkeley, California 94720, USA and Materials Sciences Division, Lawrence Berkeley National Laboratory, Berkeley, California 94720, USA

(Received 7 October 2008; revised manuscript received 18 November 2008; published 6 January 2009)

The recently discovered FeAs-based materials exhibit a $(\pi,0)$ spin density wave (SDW) in the undoped state, which gives way to superconductivity upon doping. Here we show that due to an interesting topological feature of the band structure, the SDW state cannot acquire a full gap. This is demonstrated within the SDW mean-field theory of both a simplified two-band model and a more realistic five-band model. The positions of the nodes are different in the two models and can be used to detect the validity of each model.

DOI: 10.1103/PhysRevB.79.014505 PACS number(s): 75.30.Fv, 71.18.+y, 71.10.Fd, 74.20.−z

I. INTRODUCTION

Since the discovery of superconductivity in $La_{1-x}F_xFeAs$ at $T_c=26$ K,[1] there has been mounting excitement associated both with the rapidly increasing T_c when La is substituted by other lanthanoids,[2] as well as the similarity with the cuprate superconductors. As with the cuprates, the FeAs materials are quasi-two-dimensional square-lattice-based transition-metal compounds, which are magnetically ordered at stoichiometry. On doping, in both cases, the magnetism is replaced by superconductivity.

However, there are several significant differences. Most importantly, the FeAs stoichiometric compounds are not insulating.[1,3] Also, the magnetic order here is along the $(\pi,0)$ direction and has a small moment.[4] In contrast to the cuprates, where only the $d_{x^2-y^2}$ orbital of the five Cu d orbitals is important, the multiorbital nature of the FeAs materials has been emphasized in several recent calculations.[5–7] In this paper we point out a topological aspect of the band structure closely connected with the multiorbital nature of the material that has important ramifications for the phases in this system. In particular we show that a symmetry-enforced band degeneracy at high-symmetry points in the Brillouin zone leads to a band structure with nontrivial topology. This can be quantified in terms of a "vorticity" quantum number. An example of vorticity ± 1 is the Dirac node. Here the vorticity takes on values ± 2. While such degenerate points occur in the band structure of other multiorbital systems, here they actually occur close to the Fermi level. In this paper we discuss both a simplified two-band model and a realistic five-band model where this is explicitly realized.

An important consequence of this nontrivial band topology is that it leads to an unusual spin density wave (SDW) state that is necessarily gapless. Specifically, the SDW wave vector connects hole pockets with vorticity $=\pm 2$ with electron pockets with zero vorticity. This mismatch forces nodes in the SDW gap function even in the presence of perfect nesting. Away from nesting the nodes are offset from the Fermi energy, resulting in Fermi pockets. We term such magnetic order "nodal SDW." We emphasize that the topological feature required for the nodal SDW state exists both in other simplified models in the literature[8,9] as well as first-principles band structures.[5]

In the following we first derive and study a simplified two-orbital tight-binding model motivated by the quantum chemistry. Other studies[7,8,10] have also focused on two-orbital models. However it has been argued[5,9] that one needs at least three orbitals to accurately reproduce the local-density approximation (LDA) band structure and Fermi surfaces, e.g., location of the hole pockets in the Brillouin zone. We then directly study the more general and realistic five-band model based on LDA calculation.[5] We consider the stoichiometric compound (zero doping) and study the mean-field SDW phase. This mean-field analysis confirms the existence of nodes in the SDW gap function in both models. We also established the topological stability of the nodes. The location of the nodes in momentum space and the associated Fermi-surface topologies, however, are different in the two models. This can be used to detect the validity of two-band or five-band model. A recent numerical renormalization-group study by us found precisely this nodal structure in the two-band model. The general requirements for the existence of these nodes are also discussed.

II. NODAL SDW IN THE TWO-BAND MODEL

A. Two-band microscopic model and band structure

The Fe atoms form a square lattice whose principal axes are denoted as x and y and the crystal structure axes are labeled as X and Y [Fig. 1(b)]. Let us first assume that Fe $3d_{xz}$ and $3d_{yz}$ are the relevant orbitals to describe the low-energy physics of this material. Because of the tetragonal symmetry they are locally degenerate, and we use their linear combinations $3d_{XZ}$ and $3d_{YZ}$ as our basis since they have clear symmetry when hybridized with the nearest As $4p$ orbitals. Other d orbitals will be ignored here but included in Sec. III.

In a simple chemistry picture [Fig. 1(a)] all symmetry allowed Fe $3d$-As $4p$ hybridizations are assumed to dominate over direct Fe $3d$ hybridization. This naturally leads to large nearest-neighbor (NN) orbital-changing hopping t_1 [see Fig. 1(b); note that t_1 has opposite signs between vertical and horizontal bonds] and next-NN orbital-preserving hoppings t_2 and t_2'. If we further assume that the hybridizations between $3d_{XZ,YZ}$ and $4p_Z$ [shown in Fig. 1(a)] dominate, we expect $t_2 \sim t_1 > |t_2'|$, while the direct hopping t_1' is expected to be much smaller than these three.[11] Given the empirically observed SDW order, we take $t_2 - t_2' > |t_1|$, which leads to nested electron and hole pockets at $(\pi,0)$.

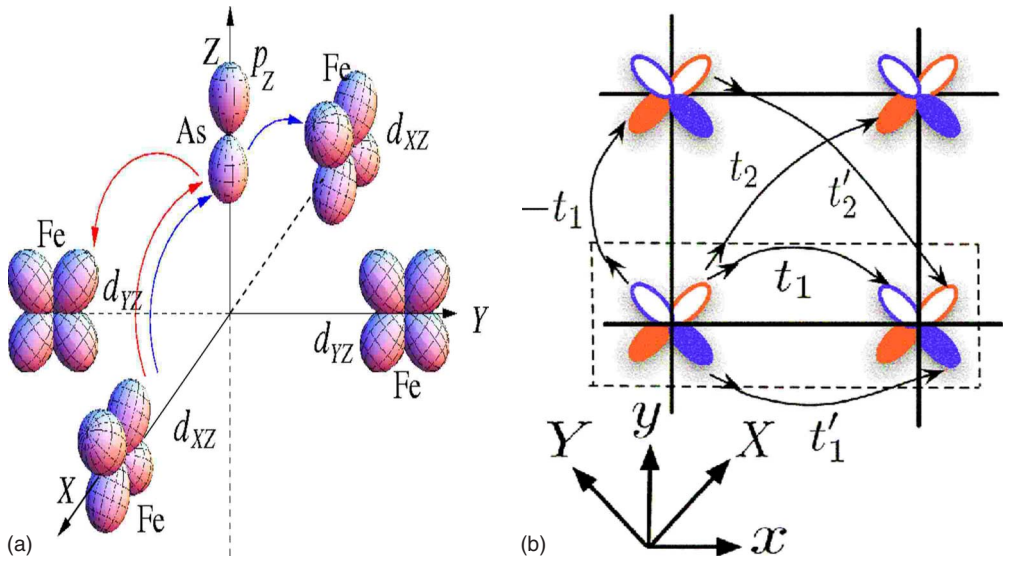

FIG. 1. (Color online) (a) The $3d_{XZ}$ and $3d_{YZ}$ orbitals of the Fe atoms and the $4p_Z$ orbital of the As atom. The blue (red) arrows represent one second-order process contributing to $t_2(t_1)$. (b) The tight-binding hoppings between the d orbitals.

To simplify the notation we will use d_1 and d_2 for electron operators associated with the XZ and YZ orbitals. The tight-binding Hamiltonian has *only* one Fe atom per unit cell, and we choose the Brillouin zone accordingly. Many other studies work with a two Fe-atom unit cell. A comparison requires an appropriate folding of the Brillouin zone of the present study. Its Fourier transform is (independent of spin)

$$H_0 = \sum_{\vec{k}} (d^\dagger_{1,\vec{k}} d^\dagger_{2,\vec{k}}) K(\vec{k}) \begin{pmatrix} d_{1,\vec{k}} \\ d_{2,\vec{k}} \end{pmatrix}, \tag{1}$$

where the sum is over $k_x \in [-\pi, \pi)$ and $k_y \in [-\pi, \pi)$ and the 2×2 matrix $K(\vec{k})$ is

$$K(k_x,k_y) = 2t_1(\cos k_x - \cos k_y)\tau_1 - 2(t_2 - t_2')\sin k_x \sin k_y \tau_3 + [2(t_2 + t_2')\cos k_x \cos k_y + 2t_1'(\cos k_x + \cos k_y)] \cdot \mathbf{1} \tag{2}$$

and $\tau_{1,2,3}$ are Pauli matrices. As argued previously we expect $t_2 > t_1 \gg t_2', t_1' > 0$. The two energy eigenvalues of Eq. (2) are

$$E_\pm(\vec{k}) = 2(t_2 + t_2')\cos k_x \cos k_y + 2t_1'(\cos k_x + \cos k_y) \pm 2\sqrt{t_1^2[\cos k_x - \cos k_y]^2 + (t_2 - t_2')^2 \sin^2 k_x \sin^2 k_y}. \tag{3}$$

In Fig. 2(a) we plot the band structure (3). At half filling the Fermi level will cut out two holelike Fermi surfaces around (0,0) and (π,π) and two electronlike Fermi surfaces around $(\pi,0)$ and $(0,\pi)$ [see Fig. 2(b)]. Note the band touchings at (0,0) and (π,π). This endows the hole Fermi surfaces with vorticity ± 2, where the spinor describing the admixture of $3d_{XZ}$ and $3d_{YZ}$ orbitals rotates twice on encircling these Fermi surfaces. The simultaneous presence of inversion and time-reversal symmetries in this band structure allows us to choose, at each k point, real spinor wave functions which are hence confined to a plane. Vorticity in this spinor field is therefore topologically protected—the singularity at the vortex center forces the orbital degeneracy at (0,0) and (π,π). In contrast, the electron Fermi surfaces are topologically trivial, with no winding as shown in Fig. 2(b). This topological characterization of the Fermi pockets is also present in more realistic LDA calculations,[5–7] although it has not been previously commented upon.

At half filling, the total electron pocket area equals the total hole pocket area. If the pockets are very small, i.e., $t_2 \approx t_1$, Taylor expansion of Eq. (3) gives four nearly circular Fermi pockets with same area. Therefore the electron and hole pockets are nested at momentum $(\pi,0)/(0,\pi)$.

It is interesting to consider for a moment the case $t_1'=0$. Then, the model decouples into two independent $t_1-t_2-t_2'$ checkerboard models. Each give rise to one hole and one-electron pocket separated by (π,π) from the other electron-hole pocket pair. Unexpectedly, the electron and hole pockets are *precisely nested* with momentum $(\pi,0)/(0,\pi)$, as long as $t_1'=0$, even when the pockets are large and noncircular. One can check that at the half-filling Fermi energy $E_F = \frac{2t_1^2}{t_2+t_2'}$, the Fermi-surface wave vectors $\vec{k}^F$ of the two bands, $E_-(\vec{k}^F) = E_F$ and $E_+(\vec{k}^F + (\pi,0)) = E_F$, satisfy exactly the same condition

$$[(t_2 + t_2')^2\cos^2 k_x^F - t_1^2][(t_2 + t_2')^2\cos^2 k_y^F - t_1^2] = (t_2 + t_2')^2(t_2 - t_2')^2 \sin^2 k_x^F \sin^2 k_y^F. \tag{4}$$

When $t_1' > 0$ the two hole pockets have different sizes. The electron pocket around $(\pi,0)$ $[(0,\pi)]$ is elongated along the k_y (k_x) direction and the perfect nesting is lost.

B. Mean-field study of the SDW order in the two-band model

Now we include on-site interactions in an extended two-band Hubbard model with $H = H_0 + H_I$ where, as in Ref. 9,

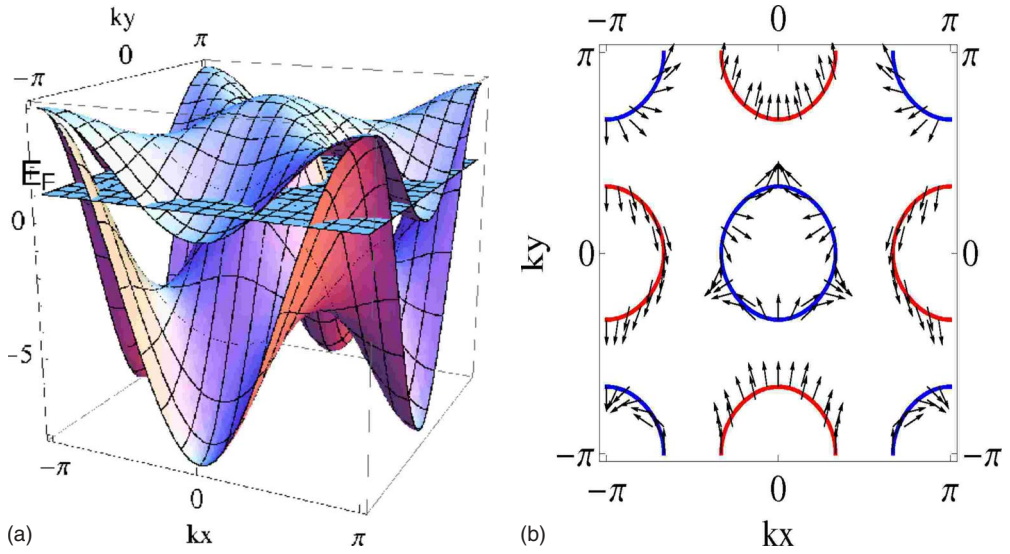

FIG. 2. (Color online) For $t_1=1$, $t_2=1.7$, $t_2'=0.3$, and $t_1'=0$ we plot (a) the dispersion $E_{\pm}(\vec{k})$ as shown in Eq. (3) together with the half-filling Fermi energy E_F and (b) the perfectly nested Fermi surfaces as given by Eq. (4) and the direction of vector $(\cos\phi_{\vec{k}}, \sin\phi_{\vec{k}})$ defined by rewriting $K(k_x,k_y)$ in Eq. (2) as $K(k_x,k_y)=a(\vec{k})\mathbf{1}+b(\vec{k})[\sin\phi_{\vec{k}}\tau_1+\cos\phi_{\vec{k}}\tau_3]$, where $b(\vec{k})>0$.

$$H_I = \frac{U}{2}\sum_i (n_{i1}^2 + n_{i2}^2) + (U-2J)\sum_i n_{i1}n_{i2} + J\sum_i^{\alpha,\beta=\uparrow,\downarrow} d_{i1,\alpha}^\dagger d_{i2,\beta}^\dagger d_{i1,\beta} d_{i2,\alpha} + J\sum_i (d_{i1,\uparrow}^\dagger d_{i1,\downarrow}^\dagger d_{i2,\downarrow} d_{i2,\uparrow} + \text{H.c.}), \quad (5)$$

where the first and second terms are the intraorbital and interorbital Coulomb repulsions. The third term is the Hund's coupling and the fourth term is the interorbital pair hopping. First-principles calculations[5] suggest that the FeAs material is in the intermediate coupling regime and we choose $t=1$, $t_1'=0.2$, $t_2=1.7$, and $t_2'=0.3$ for our hopping Hamiltonian H_0, where we estimate $t_1\sim 0.3$ eV to get the right bandwidth. Also, we use $U=4$ (1.2 eV) and $J=0.4$, which is a factor of 3 smaller than in Ref. 5 to get reasonable SDW transition temperatures and moments compatible with experiments.

For small t_1', where good nesting prevails and in the presence of repulsive onsite interactions, it is natural to consider SDW order at wave vector $(\pi,0)$. Then, $H_{\text{SDW}}=M_{ab}\Sigma_i(-)^{i_x}(d_{i,a\uparrow}^\dagger d_{i,b\uparrow}-d_{i,a\downarrow}^\dagger d_{i,b\downarrow})$, where the spin direction is assumed to be along the S_z axis. Because of the multiorbital nature of the system, different flavors of SDW are allowed, described by the Hermitian matrix M_{ab}, which may be parametrized by four real numbers $M_{ab}=[\phi_0\tau_0+\phi_1\tau_1+\phi_2\tau_2+\phi_3\tau_3]_{ab}$, where $(\tau_0)_{ab}=\delta_{ab}$. We perform the finite-temperature mean-field study by using a trial density matrix of the mean-field Hamiltonian $H_{\text{MF}}=H_0+H_{\text{SDW}}$. We construct a trial free energy based on this mean-field density matrix $F_{\text{trial}}(\phi_0,\phi_1,\phi_2,\phi_3)=F_{\text{MF}}+\langle H_I-H_{\text{SDW}}\rangle_{\text{MF}}$ where F_{MF} is the free energy of the free fermion system described by H_{MF}. The Feynman inequality[12] $F\le F_{\text{trial}}$, implies that we need to minimize F_{trial} over the mean-field parameters ϕ_i keeping the electron density fixed.

Implementing this we find that the model H_0+H_I has a unique SDW phase at low temperature characterized by $\phi_0\neq 0, \phi_1\neq 0$. The symmetry of this phase is consistent with the regular $(\pi,0)$ magnetic order depicted in Fig. 4. If we denote the order-parameter operators $\hat{m}_{ab}=d_{i,a\uparrow}^\dagger d_{i,b\uparrow}-d_{i,a\downarrow}^\dagger d_{i,b\downarrow}$, in Fig. 3(a) we plot these magnetizations as a function of temperature and it is clear that $\langle\hat{m}_{11}\rangle=\langle\hat{m}_{22}\rangle$

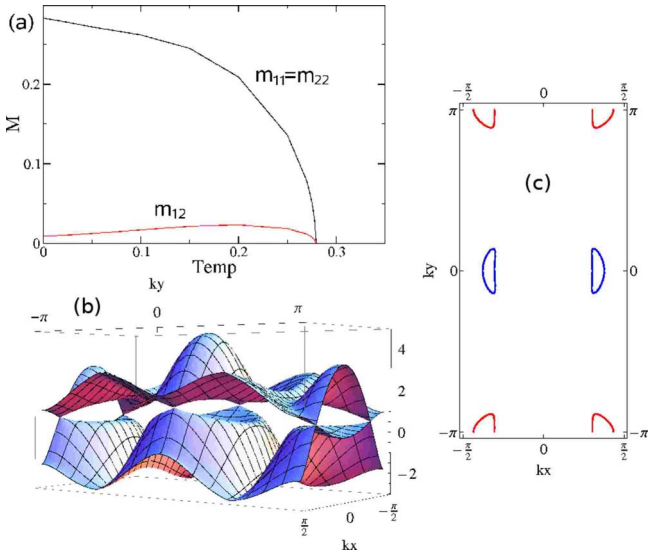

FIG. 3. (Color online) For $t_1=1$, $t_1'=0.2$, $t_2=1.7$, $t_2'=0.3$, $U=4$, and $J=0.4$ and half filling, we show (a) the magnetization $\langle\hat{m}_{11}\rangle=\langle\hat{m}_{22}\rangle$ and $\langle\hat{m}_{12}\rangle$ of the SDW phase as a function of temperature. The mean-field calculation is done on 20×20 lattice. (b) The zero-temperature SDW band structure. We plot the dispersion of two lowest-energy bands in the reduced Brillouin zone. (c) The Fermi pockets. The four nodes are not at the same energy and therefore the half-filled system has small Fermi pockets. The two nodes close to $k_y=0$ are hole doped (blue pockets) and the two nodes close to $k_y=\pi$ are electron doped (red pockets).

$\gg\langle\hat{m}_{12}\rangle$. The fact that the ϕ_2 and ϕ_3 orders are not mixed in can be understood from symmetry. Under reflections P_y about the y axis crossing the plaquette center, ϕ_0 and ϕ_1 transform differently from ϕ_3. Under time reversal, ϕ_2 order transforms differently from a SDW and in fact describes a spin-orbital locked state.

The band structure resulting from this SDW is shown in Fig. 3(d), where electron and hole pockets in the same direction as the SDW axis are visible for each pair of Fermi surfaces. Even with perfect nesting, the Fermi surfaces are *not* fully gapped; instead, there are Dirac nodes as in Fig. 3(b). In the absence of nesting these Dirac nodes are at slightly different energies and the half-filled system has small Fermi pockets. As shown below, the presence of such pockets is required under fairly general conditions. *This is the main point of the current study*. The presence of such pockets is detectable by angle-resolved photoemission spectroscopy (ARPES), and also due to the velocity anisotropy present for the nodes via conductivity measurements. Based on Drude's formula we compute the dc conductivities in x and y directions for a mean-field SDW state with nodes along the x direction and with a $T=0$ magnetic moment of $0.3\mu_B$ per Fe atom.[4] We find $\sigma_{xx}/\sigma_{yy}=6.2$. Any state with broken rotation symmetry would have conductivity anisotropy, but the large value here stems from the nodal structure discussed.

For the other SDW-type orders, ϕ_2 or ϕ_3, the nodes are along the direction orthogonal to the SDW axis. Note that although the nodal structure of our SDW gap function resembles that of a p-wave symmetry, the SDW order that we found is completely on-site and inversion symmetric.

C. No-full-gap theorem in the two-band model

In the following we argue that the Dirac nodes are topologically stable as long as the SDW order satisfies three conditions (a brief account of this argument was presented in Ref. 13): (1) collinear order (denote the magnetization direction by $\hat{n}$), (2) inversion (about the Fe site $\mathcal{I}$) symmetry, and (3) effective time-reversal symmetry $\mathcal{TR}'=\mathcal{SR}(\hat{n}\rightarrow-\hat{n})\circ\mathcal{TR}$ obtained by combining time reversal and spin reversal [$\mathcal{TR}$ is time-reversal and $\mathcal{SR}(\hat{n}\rightarrow-\hat{n})$ is the 180° spin rotation which flips the direction of magnetization]. These three conditions are naturally satisfied by a $(\pi,0)$ collinear SDW, which is consistent with experiments,[4] and the mean-field SDW that we find also satisfies these conditions.

Since we focus on the consequences of the nontrivial band structure, we begin by turning on a very weak SDW order $\hat{M}=\Sigma_{\vec{k}}\sigma^z_{\alpha\beta}M_{ab}(\vec{k})d^\dagger_{a\alpha,\vec{k}}d_{b\beta,\vec{k}+(\pi,0)}$ (where we have rotated the magnetization to the S_z direction). We therefore need to consider degenerate perturbation after folding the Brillouin zone by $(\pi,0)$. The band crossing between the two bands defined in Eq. (3), i.e., $E_-(\vec{k})$ and $E_+(\vec{k}+(\pi,0))$ forms a loop in momentum space. In the perfect nesting case these loops are identical to the electron or hole Fermi surfaces. Let us focus on the loop around (0,0) and denote the momenta on this loop by $\vec{k}^*$; thus, $E_-(\vec{k}^*)=E_+(\vec{k}^*+(\pi,0))$. Let us call the hole pocket wave functions on this loop $|\psi_h(\vec{k}^*\rangle=|\psi_-(\vec{k}^*)\rangle$ and the electron pocket wave function $|\psi_e(\vec{k}^*\rangle=|\psi_+(\vec{k}^*+(\pi,0))\rangle$. Now the degeneracy on this loop is lifted when the matrix elements of the SDW order between these two kinds of states, $m(\vec{k}^*)=\langle\psi_h(\vec{k}^*)|\hat{M}|\psi_e(\vec{k}^*)\rangle$, are nonzero.

Now, $\mathcal{I}$ symmetry requires $M_{ab}(-\vec{k})=M_{ab}(\vec{k})$. Also, given the winding of the hole Fermi-surface wave function shown in Fig. 2(b), under inversion we have $|\psi_h(-\vec{k}^*)\rangle=-|\psi_h(\vec{k}^*)\rangle$ while $|\psi_e(-\vec{k}^*)\rangle=|\psi_e(\vec{k}^*)\rangle$. Putting this together we have $m(-\vec{k}^*)=-m(\vec{k})$. In addition, $\mathcal{TR}'$ symmetry requires $M_{ab}(\vec{k})$ to be real hence so is $m(\vec{k}^*)$. We thus conclude that $m(\vec{k}^*)$ must have at least two sign changing points, K and $-K$, on the band crossing loop. These are the two of the Dirac nodes in the SDW. Similarly there are another two Dirac nodes on the band crossing loop around $(0,\pi)$.

Generically the nodes are not at the chemical potential and lead to Fermi pockets. However, a Fermi pocket deriving from a node is known, e.g., from the context of graphene, to be different from a regular Fermi pocket. In particular, electrons acquire a nontrivial Berry's phase of π on circling such a nodal pocket. We have thus argued for the stability of the Dirac nodes in SDW based on the two-band model (2). We now show that a similar result holds for the more realistic five-band model. Again the topology of the quadratic bands that touch at the Γ point is responsible for this result.

III. NODAL SDW IN THE FIVE-BAND MODEL

While the two-band model serves as a useful guide to the nontrivial physics in the SDW state, it differs from LDA calculations of the electronic structure of these materials[5] in important ways. This is easiest to see in the unfolded Brillouin-zone scheme, with a single Fe atom per unit cell (here unit translations along the x and y axes are followed by reflections in the xy plane[9]). While the two-band model has a hole pocket at $\Gamma=(0,0)$ and another one at (π,π), the LDA calculation predicts two hole pockets around the Γ point. The electron pockets, although centered on the same locations in both cases, acquire a $d_{xz}+d_{xy}$ character at $(0,\pi)$ and a $d_{yz}+d_{xy}$ character at $(\pi,0)$ in the LDA calculations. Hence they are also rather different from the two-band model that does not include the d_{xy} orbitals. A five-band hopping Hamiltonian including all the iron d orbitals is required to capture the Fermi-surface topology of the LDA calculation.

In this section we will show that even in the five-band model, the SDW is necessarily gapless (nodal SDW), despite these important differences. An important role here is played by the fact that the two hole pockets at the Γ point are derived from d_{xz} and d_{yz}, which are precisely the orbitals that enter the two-band model. In this case we will prove that there must be at least two Dirac nodes close to Fermi level in the SDW phase.

A. Mean-field study of SDW in the five-band model

We again apply the trial density-matrix method to study the $(\pi,0)$ SDW instabilities of the five-band model. We take the five-band hopping Hamiltonian H_0 from Kuroki *et al.*[5] [Eq. (1) and Table I]. We then turn on an on-site interaction in the following form:[9]

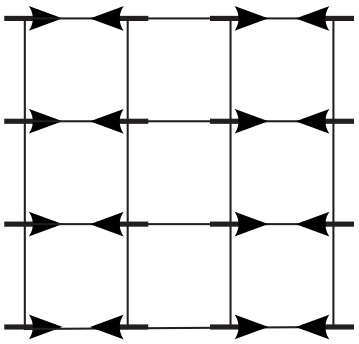

FIG. 4. The real-space pattern of the $(\pi,0)$ SDW on the Fe-atom square lattice.

$$H_I = U\sum_{i,a} n_{ia\uparrow}n_{ia\downarrow} + (U-2J)\sum_{i,a<b} n_{ia}n_{ib} + J\sum_{i,a<b}^{\alpha,\beta=\uparrow,\downarrow} d^\dagger_{ia,\alpha}d^\dagger_{ib,\beta}d_{ia,\beta}d_{ib,\alpha} + J\sum_{i,a<b}(d^\dagger_{ia,\uparrow}d^\dagger_{ia,\downarrow}d_{ib,\downarrow}d_{ib,\uparrow} + \text{H.c.}), \quad (6)$$

where $a,b=1,2,\ldots,5$ label the five orbitals $\{d_{3Z^2-R^2},d_{XZ},d_{YZ},d_{X^2-Y^2},d_{XY}\}$. We have parametrized the interorbital Coulomb interaction by $U-J$. While this is strictly expected to hold within the t_{2g} and e_g levels,[14] to reduce the number of interaction parameters, we assume it for the five-band model as well.

We only consider the on-site SDW order because the interactions are taken to be on site. Then, the $(\pi,0)$ SDW order parameter with spins assumed to point along the z axis induces the following mean-field term in the Hamiltonian:

$$H_{\text{SDW}} = \sum_i e^{i\pi i_x}\sum_{a,b=1}^{5} M_{ab}(d^\dagger_{i,a\sigma}\sigma^z_{\sigma\sigma'}d_{i,b\sigma'}), \quad (7)$$

which is parametrized by M_{ab} a Hermitian matrix with 25 real parameters. The orbital structure can lead to many different SDW states which break symmetry in different ways. Energetically, we find that the preferred state always has the same symmetry as the regular $(\pi,0)$ SDW shown in Fig. 4. That is, the state breaks time reversal $(\mathcal{TR})$ and 180° spin rotation about an axis perpendicular to the ordering direction $\mathcal{SR}$ but preserves their combination $(\mathcal{TR}')$. Also the state is invariant under inversion $\mathcal{I}$ which is a 180° rotation in the x-y plane, and reflection in the x and y axes, where the mirror plane intersects the Fe sites (P_x,P_y). At the end of this section we comment on other possible states that break different symmetries.

We now discuss details of the mean-field solution, as the on-site interaction strength is varied. Since this is not accurately known, we note the resulting ordered moment and Fermi-surface topology in each case, which may be directly compared with experiments. The Hund's coupling J is assumed to be about 20% of U.

(1) $U=1.0$ eV and $J=0.2$ eV. The temperature evolution of the net SDW magnetization $M=\langle\Sigma_a d^\dagger_{ia,\uparrow}d_{ia,\uparrow}-d^\dagger_{ia,\downarrow}d_{ia,\downarrow}\rangle$ (assuming $g=2$ this is in unit of Bohr magneton) from mean-field theory is shown in Fig. 5(a). The mean-field transition temperature obtained is $T_c=0.026$ eV while the zero-temperature magnetic moment obtained is $\sim 0.23\mu_B$. The latter is consistent with neutron-scattering experiments on LaOFeAs.[4] In Fig. 5(c) we present the Fermi surfaces of the zero-temperature half-filled SDW phase with these parameters. Note that the double degenerate point at (0,0) of the five-band hopping Hamiltonian is split into two Dirac nodes, C and C', on the k_y axis. The electron pocket at $(0,\pi)$ still intersects with Fermi level and contributes significantly to the density of states. However, on increasing the interaction strength this feature is suppressed. Stronger repulsive interactions will tend to gap out more of the Fermi surface and the electron pockets at $(0,\pi)$ can be fully gapped out. We note that the area occupied by electron pocket is 3.5% of the magnetic Brillouin zone (defined by $-\pi/2<k_x<\pi/2$ and $-\pi<k_y<\pi$). The hole pockets, of course, occupy the same area.

(2) $U=1.2$ eV and $J=0.25$ eV. In this case we obtain a somewhat larger low-temperature moment of $\sim 1.04\mu_B$. In Fig. 5(d) we plot the Fermi surfaces of the zero-temperature SDW. As compared to the previous cases, we see that the Fermi surfaces around $(0,\pi)$ disappear and the Fermi level adjusts itself to form one hole pocket around (0,0) and four electron pockets. The hole pocket occupies 2.2% of the magnetic Brillouin zone while the area of the electron pockets on the k_x axis is 0.1% each, and of those on the k_y axis is 1.0% each.

The electron pockets on k_x axis and on k_y axis are fundamentally different in that the k_x pockets arise from the Dirac nodes A and A' below them and thus protected. On the other hand the k_y pockets can be easily gapped out by turning on interactions because they are simple band bottoms [after $B(B')$ and $C(C')$ annihilate each other, which already happens in the current case].

(3) $U=1.4$ eV and $J=0.3$ eV. The zero-temperature moment is now large, $\sim 2.3\mu_B$. Now, the two electron pockets along the k_y axis are completely gapped out and we only have a small hole pocket around (0,0) and two electron pockets on the k_x axis nearby [see Fig. 5(e)]. The Fermi-surface topology and large moment obtained in this case are the closest to the LDA results.[5] The hole pockets occupy 1.4% of the magnetic Brillouin zone, while the electron pockets occupy 0.7% each.

Note that, for the larger interaction strengths, the area occupied by the residual Fermi surface in the SDW state is very small, typically a few percent. In general, interactions that drive the SDW formation would tend to lower this area. One may naturally expect that this would rapidly lead to a fully gapped state on increasing U. However, as explained in detail in Sec. III B, there is an intrinsic mechanism that blocks such a fully gapped state. A combination of symmetry and band topology necessarily leads to a gapless SDW state over a wide range of coupling strengths. This provides a "natural" protection of the small pockets that appear here and in LDA calculations, which have now been observed in magnetic oscillation experiments.[15]

Other possible orders. Before we conclude the mean-field study of SDW orders, we comment on other kinds of $(0,\pi)$ orders that could be stabilized with onsite interactions. The

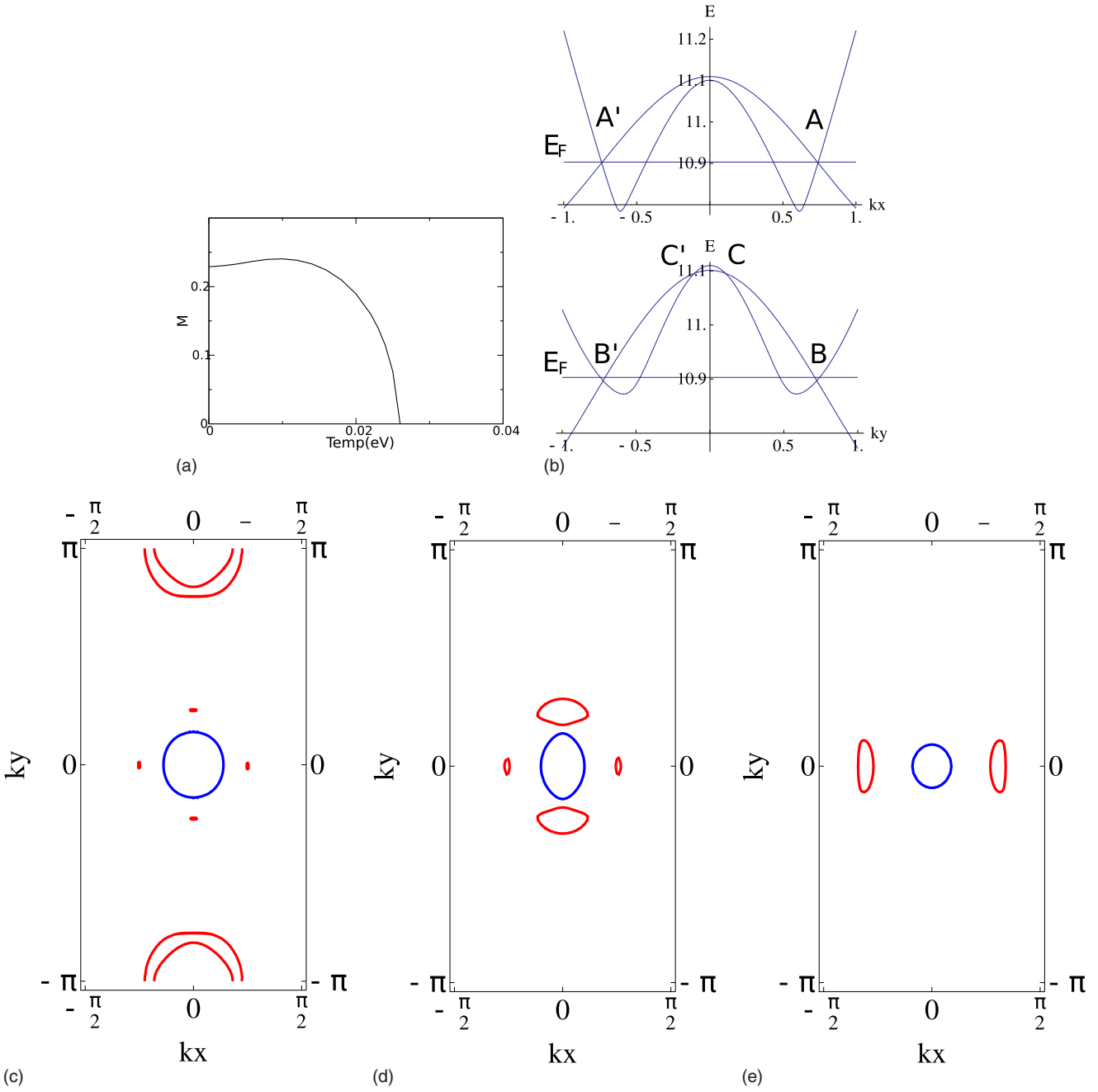

FIG. 5. (Color online) (a) Magnetization with $U=1$ eV and $J=0.2$ eV as a function of temperature (computation is performed on a 40×40 lattice with periodic boundary). (b) $T=0$ dispersion in this SDW state showing the two low-energy bands along k_x and k_y axes around (0,0). There are four nodes close to Fermi energy: A and A' on the k_x axis and B and B' on the k_y axis. The double degenerate point at (0,0) of the five-band hopping Hamiltonian is split into two Dirac nodes, C and C', on the k_y axis. We also plot the zero-temperature Fermi surfaces (blue pockets are holelike and red pockets are electronlike) with (c) $U=1$ eV and $J=0.2$ eV, (d) $U=1.2$ eV and $J=0.25$ eV, and (e) $U=1.4$ eV and $J=0.3$ eV.

25 parameter M_{ab} matrix admits a plethora of different orders, which may be separated into the following four classes, according to the symmetries of the resulting SDW Hamiltonian H_{SDW}: (i) $\mathcal{TR}'$ even, $\mathcal{I}$ even, and P_x, P_y even (six parameters). This is the SDW state that was considered above. The no-full-gap theorem discussed below applies to this case. (ii) $\mathcal{TR}'$ even, $\mathcal{I}$ even, and P_x, P_y odd (three parameters). (iii) $\mathcal{TR}'$ even and $\mathcal{I}$ odd (six parameters). (iv) $\mathcal{TR}'$ odd (ten parameters). This case is rather exotic because $\mathcal{TR}$ is even but $\mathcal{SR}$ is odd. This is similar to the symmetry of a spin-Hall insulator.[16]

To compare the relative stabilities of these different states, we choose $U=1$ eV and $J=0.2$ eV and first perform an unbiased minimization of all the 25 parameters. We find that class (i) is always the low-free-energy solution and with the highest $T_c=0.026$ eV. Even if we suppress order parameter (i) by hand, we find that the system has no instability toward (ii), (iii), and (iv) down to 0.0001 eV. (Computations were

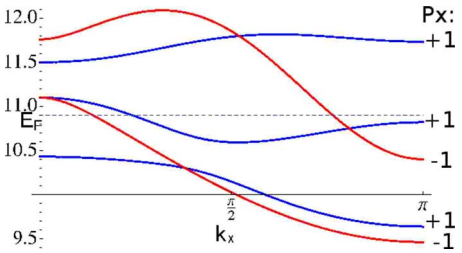

FIG. 6. (Color online) We present the P_x eigenvalues (blue for +1 and red for −1) of the five bands along k_x axis.

performed on a 40×40 lattice with periodic boundary.) We conclude that SDW (i) is the low-free-energy phase in model (6) and is consistent with the ordered pattern observed in experiments. Hence, we do not pursue studying these other kinds of SDW order.

B. No-full-gap theorem in the five-band model

In this section we explain why the nodal SDW found in the mean-field study appears. We assume that the SDW has the symmetries in (i) above, as found in mean-field theory. Briefly, we use reflection symmetry along $k_x=0$ and $k_y=0$ to label bands with a reflection eigenvalue. Bands connected to the electron pocket and a hole pocket are forced to have opposite eigenvalues and hence do not split in the SDW state along these lines, leading to a gapless state. An important role is played by the band touching at the $k=(0,0)$ point, as in the two-band model. While this reasoning holds for weak SDWs, we extend it to include strong SDW instabilities, where the location of the band intersections can migrate to the Γ point, even in this case so we show that at least two gapless Dirac nodes will remain.

Weak SDW limit. The reflections P_x and P_y through mirror planes along xz and yz, which pass through the Fe atoms, act on the orbital basis of $\{d_{3Z^2-R^2},d_{XZ},d_{YZ},d_{X^2-Y^2},d_{XY}\}$ as follows:

$$T_{P_x}:\begin{pmatrix}1&0&0&0&0\\0&0&1&0&0\\0&1&0&0&0\\0&0&0&-1&0\\0&0&0&0&1\end{pmatrix},\quad T_{P_y}:\begin{pmatrix}1&0&0&0&0\\0&0&-1&0&0\\0&-1&0&0&0\\0&0&0&-1&0\\0&0&0&0&1\end{pmatrix}. \tag{8}$$

Spin is left invariant as we ignore spin-orbit interactions. We first consider the P_x reflection symmetry. Along k_x axis the Bloch Hamiltonian is P_x symmetric and the wave function should be eigenstates of P_x with eigenvalues of ±1. We thus can simply present the eigenvalue of P_x of each band as shown in Fig. 6. If we focus on the three bands close to Fermi level, we find that the electron pocket is P_x odd, the large hole pocket is P_x even, and the small hole pocket is P_x odd. Since the relevant SDW orders are P_x even, the SDW-induced gap along k_x axis between the electron pocket and the large hole pocket must vanish; i.e., there is a band crossing. These are labeled A and A' in the example of Fig. 5(b). We note that the bands corresponding to the large hole pocket and the small hole pocket must have opposite P_x eigenvalues and as a result the nodes must exist no matter whether the electron pocket is P_x even or odd. The simplest way to understand this is to note that the double degenerate wave functions at (0,0) are nothing but d_{xz} and d_{yz}. Hence, these band touchings play a crucial role here, as in the two-band model.

Similarly there must be nodes also along the k_y direction by studying the P_y eigenvalues along the k_y axis. We find that the electron pocket is P_y odd, while the large hole pocket is P_y even, and small hole pocket is P_y odd. Therefore we expect that the SDW gap vanishes along k_y direction between the electron pocket and the large hole pocket as well. These are labeled B and B' in the example of Fig. 5(b). Hence, in the limit of a weak SDW, the Fermi energy will inevitably cross at least one of the protected bands, and a full gap cannot result. Note that the existence of pockets is independent of how good the nesting is, in contrast to conventional SDWs which are gapless only due to the absence of nesting. A further distinction is that some of the gapless pockets in our case result from Dirac nodes.

Strong SDW. The above four band crossings are obtained assuming that the SDW is a weak perturbation. If SDW is strong can these nodes annihilate and lead to a fully gapped SDW? Note that, in the presence of $\mathcal{TR}'$ and $\mathcal{I}$ symmetry, a band crossing can only be removed via annihilation with a partner. Since the band crossings appear close to the Γ point, it is particularly important to address whether they can annihilate by coming together at that point. For completeness, it is important to note that in addition to the four band crossings discussed above, there are two additional ones that arise when C_{4v} is broken in the SDW state. The double vortex at (0,0) is split into two Dirac nodes with the same chirality when the SDW order is turned on. Therefore there are totally six band crossings around (0,0) in the weak SDW limit [labeled as A,B,C and A',B',C' in the mean-field example of Fig. 5(b)]. In the Appendix we prove an important theorem based on a topological argument ensuring that these six nodes can never annihilate in pairs at (0,0). We show that this is ensured by the fact that the two wave functions at (0,0), which correspond to d_{XZ},d_{YZ} are both odd under inversion $\mathcal{I}$. The nodes can only annihilate in sets of four. We conclude that there must be at least two Dirac nodes left. This result is topologically stable. Indeed, on going to stronger interaction strengths this is the state realized in our mean-field study, e.g., in Fig. 5(f). In that case the two left-over Dirac nodes are along the k_x axis.

Now we compare the nodal SDW in two-band model and five-band model. One main difference is that the Fermi-surface topologies and shapes are quite different. In particular in the five-band model there may not be a large anisotropy of conductivity as in the two-band model because at least there is a rather circular hole pocket around (0,0). The positions of Dirac nodes and Fermi-surface topologies, which may be easily measured by single-crystal ARPES, can serve as a way to directly detect the validity of two-band model or five-band model.

IV. CONCLUSIONS

In this paper we studied the spin density wave (SDW) ground state of the undoped FeAs compound. We find that the combination of physical symmetry and the topology of the band structure naturally stabilizes a gapless SDW ground state with Dirac nodes. We first study the popular two-band model due to its simplicity, where this mechanism is manifested. We also study the more realistic five-band model, where the same results obtained. These two rather different models share a key topological feature of the band structure: the double degeneracy at $\vec{k}=(0,0)$ enforces a wave function winding around this point in the Brillouin zone.

In both models we perform the mean-field study allowing for all possible collinear magnetic orders at $(\pi,0)$ and find the inversion and reflection parities of the lowest-energy magnetic ordered phase. We then show that the SDW ground state in both models has stable Dirac nodes protected by the inversion symmetry and the topology of the band structure. These Dirac nodes are close to Fermi level and thus may be directly observable in ARPES experiments and might also control the low-energy thermodynamic and transport properties of compound. They arise due to the vanishing of the SDW matrix elements along a high-symmetry line in the Brillouin zone, which leaves the Fermi surfaces ungapped in this direction. We also proved a general result on the stability of Dirac nodes against pairwise annihilation in an inversion symmetric system (Appendix) which may be applied to more general situations. While strong interactions tend to increase the SDW gap and reduce the Fermi pocket area, the nodal nature of the SDW does not allow a full gap to open over a wide range of interaction strengths. Hence, one expects to be left with small residual Fermi-surface pockets, which naturally explains the small Fermi surface areas (0.52% and 1.38% of the Brillouin zone with two Fe atoms per unit cell) observed in magnetic oscillation experiments.[15]

Although we find stable Dirac nodes in the SDW ground state in both the two- and five-band models, the number and the locations of the Fermi pockets are different. These differences can serve as ways to determine which is a better model of the material. Effective low-energy theories of the FeAs materials should ideally incorporate the nodal nature of the SDW state, which may also have important consequences for other phases in this system.

ACKNOWLEDGMENTS

We acknowledge useful discussions with Cenke Xu. A.V. would like to thank Leon Balents for stimulating conversations, Steve Kivelson for pointing out Ref. 1 at an early stage, and support from LBNL DOE Contract No. 504108 and NSF Contract No. DMR 0645691. D.H.L. was supported by DOE under Contract No. DE-AC02-05CH11231.

APPENDIX: ANNIHILATION CONDITION FOR DIRAC NODES

We consider the general question of when a pair of Dirac nodes can come together and annihilate to give rise to a nonsingular band structure. We assume the existence of both *time reversal* and *inversion* symmetries. We consider the case where a pair of Dirac nodes comes together at a point $\mathcal{M}$ in momentum space—which is constrained by the symmetries above to be invariant under inversion. When the Dirac nodes are near this point, we can restrict attention to just the two bands that make up these nodes. At the $\mathcal{M}$ point, they can be labeled by their eigenvalues under inversion $I_1 = \pm 1$ and $I_2 = \pm 1$. Below we show that only if $I_1 I_2 = -1$ can the pair of nodes annihilate. Otherwise, they necessarily lead to a band touching with quadratic dispersion at the $\mathcal{M}$ point when they are brought together.

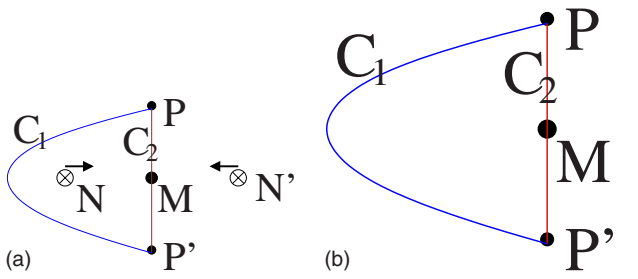

FIG. 7. (Color online) We show the paths C_1 and C_2 connecting two points P and P' which are inversion images of each other (a) before annihilation and (b) after annihilation. C_2 crosses the inversion symmetric point M, and before annihilation C_1+C_2 encloses one single Dirac node N.

To derive this result, we use a Berry's phase formula to fix the inversion eigenvalue of the $\mathcal{M}$ point states before and after node annihilation. This places the required constrain on the inversion eigenvalues if the nodes are to annihilate. We first define the inversion parity $\sigma(C)$ of a half loop C connecting two points P and P', which are mapped to one another by inversion. We start with the wave function of one of the bands at P, $|\Psi_P\rangle$, which can be taken to be real given that we have both time reversal and inversion symmetries. This is evolved adiabatically along the contour C to give the real wave function $|\Psi'_P\rangle$ at point P'. Clearly this is an eigenstate of the Bloch Hamiltonian at this point in the Brillouin zone. A separate way to obtain the eigenstate at P' is to apply the inversion operation on the state at P, $I|\Psi_P\rangle$. Again, the inversion operation can be constructed to yield a real wave function. Hence, these two wave functions can at most differ by a sign,

$$|\Psi'_P\rangle = \sigma(C) I |\Psi_P\rangle, \tag{A1}$$

which is the inversion parity $\sigma(C)$ of the curve C. Note that since $I^2=1$, $\sigma(C)$ is independent of the direction of C. Although it depends on the band index, the band label is suppressed for clarity.

Now consider two nodes N and N' being brought together at $\mathcal{M}$ and choose two points P and P' along the perpendicular direction of this path. As shown in Fig. 7 we choose two paths C_1 and C_2 connecting P and P'. Initially, C_1+C_2 encloses a single Dirac node at N, and as a result we must have $\sigma(C_1)\sigma(C_2)=-1$ because the wave function must wind by π around a Dirac point. Now *assume* that the nodes annihilate on being brought together. Now, C_1+C_2 encloses no singularity, so the inversion parities $\sigma'(C)$ after this operation sat-

isfy $\sigma'(C_1)\sigma'(C_2)=+1$. However, since the wave functions along C_1 evolve smoothly during the annihilation we have $\sigma'(C_1)=\sigma(C_1)$. Therefore we must have $\sigma'(C_2)=-\sigma(C_2)$. Note that, by shrinking the curve C_2, we can approach the $\mathcal{M}$ point. Then, the inversion parity of the curve simply becomes the eigenvalue under inversion of the wave function at the $\mathcal{M}$ point, (I_1,I_2). Therefore we conclude that in the node annihilation process, the inversion eigenvalue of each of the two states at the $\mathcal{M}$ point changes sign. This is only possible if they have opposite signs to begin with, $I_1I_2=-1$. In that case they can simply pass through each other, and the net result will be a sign change in the inversion eigenvalue of the higher- and lower-energy states. However, if they both have the same sign, $I_1I_2=+1$, it is not possible to affect a sign change. In this case, our assumption that the nodes annihilate is invalid—in fact a pair of bands with quadratic dispersion will touch at the $\mathcal{M}$ point.

If the two bands have opposite inversion eigenvalues, then the inversion matrix in the two bands is τ^3, and the inversion symmetric real Hamiltonian around M must be able to expand as $(a\delta k_x)\tau^1+(\epsilon+b\delta k_x^2+c\delta k_y^2+d\delta k_x\delta k_y)\tau^3$ to the quadratic order after choosing the k_x axis to be along direction connecting the two nodes. We immediately see that depending on the sign of ϵ, the Hamiltonian either has two- or zero-band touching nodes. This indicates that if the two bands have opposite inversion eigenvalues, the two nodes can always annihilate at $\mathcal{M}$.

Finally we note that the SDW state in the five-band model meets the conditions required for the above analysis to hold. Inversion $\mathcal{I}$ is a symmetry of the system, and the role of time reversal is played by $\mathcal{TR}'=\mathcal{SR}(\hat{n}\rightarrow-\hat{n})\circ\mathcal{TR}$ (defined in text) symmetric system, where $\hat{n}$ is the direction of collinear SDW. Let us choose the orbital basis d_a $(a=1,\ldots,n)$ to be eigenfunctions of inversion and label the eigenvalues to be I_a. We then define the $\mathcal{I}\circ\mathcal{TR}$ even basis $\tilde{d}_a$ in the following fashion: if $I_a=1$ then $\tilde{d}_a=d_a$, and if $I_a=-1$ then $\tilde{d}_a=id_a$. For a collinear SDW with $\mathcal{TR}'$ symmetry the Hamiltonian in $\tilde{d}_a$ is purely real, and so are the eigenfunctions in the momentum space. In this basis, the arguments presented above can be made, leading to the conclusion that a pair of Dirac nodes cannot be annihilated at the Γ point. Hence, since we begin with six nodes in all, there will always be a leftover pair that is stable.

[1] Y. Kamihara, T. Watanabe, M. Hirano, and H. Hosono, J. Am. Chem. Soc. **130**, 3296 (2008).

[2] G. F. Chen, Z. Li, G. Li, J. Zhou, D. Wu, J. Dong, W. Z. Hu, P. Zheng, Z. J. Chen, H. Q. Yuan, J. singleton, J. L. Luo, and N. L. Wang, Phys. Rev. Lett. **101**, 057007 (2008); H. H. Wen, G. Mu, L. Fang, H. Yang, and X. Zhu, Europhys. Lett. **82**, 17009 (2008); X. H. Chen, T. Wu, G. Wu, R. H. Liu, and H. Chen, Nature (London) **453**, 761 (2008); G. F. Chen, Z. Li, D. Wu, G. Li, W. Z. Hu, J. Dong, P. Zheng, J. L. Luo, and N. L. Wang, Phys. Rev. Lett. **100**, 247002 (2008); Z.-A. Ren, J. Yang, W. Lu, W. Yi, X. L. Shen, Z. C. Li, G. C. Che, X. L. Dong, L. L. Sun, F. Zhou, and Z. X. Zhao, Europhys. Lett. **82**, 57002 (2008); Z.-A. Ren, J. Yang, W. Lu, W. Yi, G. C. Che, X. L. Dong, L. L. Sun, F. Zhou, and Z. X. Zhao, Mater. Res. Innovations **12**, 105 (2008); P. Cheng, L. Fang, H. Yang, X. Y. Zhu, G. Mu, H. Q. Luo, Z. S. Wang, and H. H. Wen, Sci. China, Ser. G **51**(6), 719 (2008).

[3] J. Dong, H. J. Zhang, G. Xu, Z. Li, G. Li, W. Z. Hu, D. Wu, G. F. Chen, X. Dai, J. L. Luo, Z. Fang, and N. L. Wang, Europhys. Lett. **83**, 27006 (2008).

[4] C. de la Cruz, Q. Huang, J. W. Lynn, J. Li, W. R. Ii, J. L. Zaretsky, H. A. Mook, G. F. Chen, J. L. Luo, N. L. Wang, and Pengcheng Dai, Nature (London) **453**, 899 (2008); M. A. McGuire, A. D. Christianson, A. S. Sefat, B. C. Sales, M. D. Lumsden, R. Jin, E. A. Payzant, D. Mandrus, Y. Luban, V. Keppens, V. Varadarajan, J. W. Brill, R. P. Hermann, M. T. Sougrati, F. Grandjean, G. J. Long, Phys. Rev. B **78**, 094517 (2008).

[5] D. J. Singh and M. H. Du, Phys. Rev. Lett. **100**, 237003 (2008); K. Haule, J. H. Shim, and G. Kotliar, *ibid.* **100**, 226402 (2008); I. I. Mazin, D. J. Singh, M. D. Johannes, and M. H. Du, *ibid.* **101**, 057003 (2008); K. Kuroki, S. Onari, R. Arita, H. Usui, Y. Tanaka, H. Kontani, and H. Aoki, *ibid.* **101**, 087004 (2008).

[6] X. Dai, Z. Fang, Y. Zhou, and F. C. Zhang, Phys. Rev. Lett. **101**, 057008 (2008); H.-J. Zhang, G. Xu, X. Dai, and Z. Fang, arXiv:0803.4487 (unpublished); Z.-J. Yao, J.-X. Li, and Z. D. Wang, arXiv:0804.4166 (unpublished); V. Cvetkovic and Z. Tesanovic, arXiv:0804.4678 (unpublished).

[7] Q. Si and E. Abrahams, Phys. Rev. Lett. **101**, 076401 (2008).

[8] S. Raghu, X. L. Qi, C. X. Liu, D. J. Scalapino, and S. C. Zhang, Phys. Rev. B **77**, 220503(R) (2008).

[9] P. A. Lee and X.-G. Wen, Phys. Rev. B **78**, 144517 (2008).

[10] Tao Li, J. Phys.: Condens. Matter **20**, 425203 (2008).

[11] In Ref. 10 similar reasoning is employed but $3d_{XZ,YZ}$-$4p_Z$ hybridization is neglected which we believe is dominant. The parameters of Ref. 8 are related to ours via $t_1=(t_2-t_1)/2$, $t_1'=-(t_1+t_2)/2$, $t_2=t_4-t_3$, and $t_2'=-t_4-t_3$.

[12] R. P. Feynman, *Statistical Mechanics* (Addison-Wesley, Reading, MA, 1998).

[13] F. Wang, H. Zhai, Y. Ran, A. Vishwanath, and D. H. Lee, arXiv:0805.3343 (unpublished).

[14] C. Castellani, C. R. Natoli, and J. Ranninger, Phys. Rev. B **18**, 4945 (1978); Raymond Frésard and Gabriel Kotliar, *ibid.* **56**, 12909 (1997).

[15] S. E. Sebastian, J. Gillett, N. Harrison, P. H. C. Lau, C. H. Mielke, and G. G. Lonzarich, J. Phys.: Condens. Matter **20**, 422203 (2008).

[16] C. L. Kane and E. J. Mele, Phys. Rev. Lett. **95**, 226801 (2005).